Mon. Not. R. Astron. Soc. **000**, 1–12 (2013) Printed 28 July 2014 (MN LATEX style file v2.2)

Planetary nebulae: the universal mass-metallicity relation for Local Group dwarf galaxies and the chemistry of NGC 205⋆

Denise R. Gonçalves[1,2]†, Laura Magrini[3], Ana M. Teodorescu[4,5], Carolina M. Carneiro[1]
[1] *Observatório do Valongo, Universidade Federal do Rio de Janeiro, Ladeira Pedro Antonio 43, 20080-090 Rio de Janeiro, Brazil*
[2] *Instituto de Astrofísica de Canarias (IAC), E-38200 La Laguna, Tenerife, Spain*
[3] *INAF - Osservatorio Astrofisico di Arcetri, Largo E. Fermi 5, I-50125 Firenze, Italy*
[4] *Consiglio Nazionale delle Ricerche, Pisa, Italy*
[5] *Institute for Astronomy, University of Hawaii, USA*

arXiv:1407.6864v1 [astro-ph.GA] 25 Jul 2014

Accepted ?. Received ?; in original form ?

ABSTRACT

Here we study 16 planetary nebulae (PNe) in the dwarf irregular galaxy NGC 205 by using GMOS@Gemini spectra to derive their physical and chemical parameters. The chemical patterns and evolutionary tracks for 14 of our PNe suggest that there are no type I PNe among them. These PNe have an average oxygen abundance of 12+log(O/H)=8.08±0.28, progenitor masses of 2-2.5 $M_{\odot}$ and thus were born ∼1.0-1.7 Gyr ago. Our results are in good agreement with previous PN studies in NGC 205. The present 12+log(O/H) is combined with our previous works and with the literature to study the PN metallicity trends of the Local Group (LG) dwarf galaxies, in an effort to establish the PN luminosity- and mass-metallicity relations (LZR and MZR) for the LG dwarf irregulars (dIrrs) and dwarf spheroidals (dSphs). Previous attempts to obtain such relations failed to provide correct conclusions because were based on limited samples (Richer & McCall 1995; Gonçalves et al. 2007). As far as we are able to compare stellar with nebular metallicities, our MZR is in very good agreement with the slope of the MZR recently obtained for LG dwarf galaxies using spectroscopic stellar metallicities (Kirby et al. 2013). Actually, we found that both dIrr and dSph galaxies follow the same MZR, at variance with the differences claimed in the past. Moreover our MZR is also consistent with the global MZR of star-forming galaxies, which span a wider stellar mass range (∼ 10^6- 10^{11}M⊙).

Key words: Galaxies: abundances - evolution - Local Group - Individual (NGC 205); ISM: Planetary Nebulae

1 INTRODUCTION

Dwarf galaxies are the most numerous system in the Universe, and most of them are found in galaxy groups. Dwarfs in the Local Group (LG) are excellent laboratories to study galaxy evolution. Planetary nebulae (PNe) are among the brightest resolved stars in LG dwarf galaxies. Their strong emission line features allow us to study the late evolutionary stages of stars with low and intermediate masses (∼1-8 M⊙). They are also tracers of the star formation history and chemical enrichment in an age range from ∼1 to 10 Gyr ago.

In a series of previous papers (Magrini et al. 2005, Leisy et al. 2005, 2006, Gonçalves et al. 2007, Magrini & Gonçalves 2009, Gonçalves et al. 2012) we have investigated the chemical properties of the emission-line populations of LG dwarf galaxies, observing H II regions and PNe in star-forming galaxies such as dwarf irregulars (dIrrs) and only PNe in quiescent galaxies, such as dwarf spheroidals (dSphs).

1.1 NGC 205 and its PN population

In the present paper we discuss our Gemini Multi-Object Spectrographs North (GMOS-N) spectroscopic observations of the PN population in the dwarf galaxy NGC 205, the

⋆ Based on observations obtained at the Gemini Observatory, which is operated by the Association of Universities for Research in Astronomy, Inc., under a cooperative agreement with the NSF on behalf of the Gemini partnership.

† E-mail: denise@astro.ufrj.br

brightest early-type dwarf satellite of Andromeda (M31). NGC 205 is of particular importance among the low surface brightness galaxies in the LG because of its interesting star formation history and several indications of a tidal encounter with its massive companion M31. Being located at a projected distance of 42 kpc from M31, NGC 205 is one of the closest M31 satellites. The star formation history in NGC 205 has been studied extensively (e.g,. Bertola et al. 1995; Davidge 2003): an old stellar population (10 Gyr; Bica, Alloin & Schmidt 1990) dominates the overall stellar content and a plume of bright blue stars, later identified as star clusters (Cappellari et al. 1999), was found in the central region (Baade 1944; Hodge 1973). Davidge (2003), studying the population of asymptotic giant branch (AGB) stars, noted that the multiple episodes of star formation (SF) may have occurred in NGC 205's most central regions, with a time spacing compatible with its orbital period (Cepa & Beckman 1988). Therefore, tidal interactions with M31 could have triggered the latest episodes of SF. However, recent observations with HST point towards a constant star formation rate (SFR, Monaco et al. 2009), at least during the last ∼300 Myr, as if NGC 205 was approaching M31 for the first time (see also Howley et al. 2008). In addition to young stars, NGC 205 also contains gas (H I + CO; 1.5×10^6 M$\odot$, e.g. Young & Lo 1997). A new estimate of the total gas content has been provided by De Looze et al. (2012), enlarging the estimates from previous measurements, but confirming the problem of missing interstellar medium mass, i.e., an inconsistency of the measured gas mass when contrasted with theoretical predictions of the current expected gas content in NGC 205 ($>10^7$ M$\odot$). This deficiency was explained with an efficient supernovae feedback able to expel gas/dust from the inner, star-forming regions of NGC 205. The population of PNe in NGC 205 was first identified by Ford et al. (1977) and later by Ciardullo et al. (1989). Corradi et al. (2005) recovered 20 of the previously known candidates and added another 55 new PNe to the candidate population, some of them actually belonging to the halo of M31. Richer & McCall (2008) presented chemical abundances for thirteen among the brightest PNe of NGC 205, based on spectroscopic data obtained at the Canada-France-Hawaii Telescope. From their chemical composition they argued that the PN progenitors of the galaxy are typically low mass stars, with M∼1.5 M$\odot$ or less. Having such low mass progenitors, they likely do not dredge up significant quantities of oxygen, and thus these PNe can be considered good tracers of the interstellar medium (ISM) from which they were born.

1.2 The mass-metallicity relation

The second aim of the present paper is to establish the luminosity-metallicity relation (LZR), as well as the mass-metallicity relation (MZR), for the dSphs and dIrrs of the Local Group, in a fully homogeneous way. On the shoulders of the latter lies the key to disentangle possible differences in star-forming and non star-forming dwarf galaxies, as claimed long ago by Skillman et al. (1989) and Kormendy & Djorgovski (1989).

A serious problem for deriving the above relations is that the metallicities are measured using different diagnostics in star-forming and non-star forming galaxies. The metallicity of the star-forming dIrrs is obtained by measuring the O/H of their H II regions, whereas dSphs are gas and dust free –dominated by the old stellar population– so, the derived value is the [Fe/H][1] from red giants or other bright stars. Following Mateo (1998), the oxygen abundances can be converted in iron metallicity, although the assumptions about the [O/Fe] are very uncertain, since the latter ratio depends on the star formation history (SFH) of the galaxies (Gilmore & Wyse 1991). Therefore, only populations present in both dSphs and dIrrs types of galaxies can be safely applied for such a study. In this context PNe are the ideal population to measure the metallicity of the dwarf spheroidals and irregulars, as proposed by Richer & McCall (1995), and actually successfully applied by these authors, as well as by Gonçalves et al. (2007). Moreover, using the PN population, both groups found that the dSphs LZR presented a significant offset from the dIrrs, with PNe in dSphs having higher O/H than those of the dIrrs. Gonçalves et al. (2007) had also compared the O/H of H II regions of a sample of dIrrs, showing no important difference between these abundances. Kormendy & Djorgovski (1989) had proposed an evolutionary relation among the two morphological types of dwarfs, with the dSph galaxies being formed through the removal of the gas in dwarf irregulars, either through ram pressure stripping, supernova driven winds or star formation. Trying to shed light on this matter, Gonçalves et al. (2007) added their own measurement for NGC 147 to the data collected from literature and pointed out that the LZR of dSphs did not exclude their formation from old dwarf irregular galaxies, but it did exclude their formation from the present time dIrrs, since the differences between their metallicities were already present in the old PNe populations of both types. The LZR offset, then, indicates a faster enrichment of dSphs and the different SFH for these two types of galaxies are also discussed by Grebel (2005).

By combining photometric and spectroscopic stellar metallicity estimates for red giant branches, Grebel et al. (2003) showed the existence of an offset between the LZR of dSphs and dIrrs. These relations are such that dSphs have higher mean stellar metallicities for a fixed optical luminosity, as in the case of the above discussed PN LZR. They also found that the same offset persists when the comparison is restricted to the galaxies old stellar populations. Grebel et al. (2003; also see Koleva et al. 2013) highlighted the transition-type dwarfs –dwarfs with mixed dIrr/dSph morphologies, low stellar masses, low angular momentum, and H I contents of at most a few 10^6 M$_\odot$, which closely resemble dSphs if their gas were removed–, and concluded that these transition objects are likely dSph progenitors. However, in more recent works based on stellar metallicities (Lee et al. 2008; Kirby et al. 2013) the above offset raised some questions, since the latest studies, more consistently, only use spectroscopic stellar metallicities. The caveat in Grebel et al. (2003) approach was precisely the fact that the colors of red giants are subject to the age-metallicity degeneracy (Salaris & Girardi 2005; Lianou et al. 2011). In Lee et al. (2008) the metallicities of the dIrrs from RGB were reanalysed, and showed to be 0.5 dex higher than in Grebel et al. (2003), so vanishing the previously found offset. Kirby et

[1] Brackets indicate that the metallicity is given with respect to the solar metallicity.

al. (2013) used spectroscopic metallicities of individual stars in seven gas-rich dwarf irregular galaxies, and found that dIrrs obey the same mass-metallicity relation as the dSph satellites of both the Milky Way and M31. Moreover, their MZR is roughly continuous with the stellar mass metallicity relation for galaxies as massive as M = 10^{12} $M_{\odot}$.

On the controversial trends given by the latest stellar LZR/MZR (Kirby et al. 2013) as compared to the PNe LZR (Gonçalves et al. 2007) resides our motivation to revisit such relation from the PN population.

1.3 Outline of the present work

Though in the present paper we present our new spectroscopic observations of 22 candidate PNe in NGC 205 –for which we confirm the PN status of 19–, our work's major aims can be summarised as follows.

i) By deriving the chemical composition of dwarf galaxies from PNe (and H II regions, whenever possible), so setting constraints to galaxy formation and evolution, we have the unique possibility to determine directly the chemical composition of the ISM in different epochs than the present one, such as, for example, at the time of the formation of the PN progenitors.
ii) Studying the stellar nucleosynthesis of low- and intermediate-mass stars in different conditions and at different metallicity environments.
iii) Deriving, in a homogeneous way, the metallicity –as traced, e.g., by the oxygen abundance–, in both dIrrs and dSphs. This approach allows us to derive the luminosity (and mass)-metallicity relation for all dwarf galaxies, in a fully homogeneous way, to disentangle possible differences in this relation for star-forming and non star-forming galaxies, as claimed in the past.

The paper is structured as follows. The acquisition and reduction of the observational data (imaging and spectroscopy) is discussed in Section 2. The analysis and interpretation of the spectroscopy for the 19 PNe we observed are given in Section 3, where electron densities and temperatures, as well as ionic and total abundances are presented, for a sub-sample of these PNe. In this section also appears a discussion of spectroscopic results in terms of abundances patterns and the PN progenitors age and masses. This is followed, in Section 4, by the determination of the luminosity-metallicity relationship and the mass-metallicity relationship for the LG dIrrs and dSphs, as given by their PN population (in sub-sections 4.1 and 4,2 respectively). In Section 5 we highlight the principal results of all the previous sections of the paper.

2 OBSERVATIONS: DATA ACQUISITION AND REDUCTION

We obtained pre-imaging of NGC 205 with GMOS at Gemini North telescope in 2010 observing two fields of 5.5′×5.5′ each. In July 9 we observed Field-1 (centred at 00:40:12.50/+41:40:03) and September 2-3 Field-2 (00:40:10.50/+41:43:47.0). We used the on- and off-band imaging technique to identify PNe and other emission-line objects with two filters: [O III], OIII_G0318, and [O III]-Continuum, OIII_G0319, whose central λ and width are 499 nm/5 nm, and 514 nm/10 nm, respectively. We obtained three exposures of 540(810) s using the on-band(off-band) filter. We used the two combined narrow-band frames to build an [O III] continuum-subtracted image per field, from which we identified a total of 37 objects to be spectroscopically observed, including previously known PNe and other emission-line objects. See Table 1 and Figure 1.

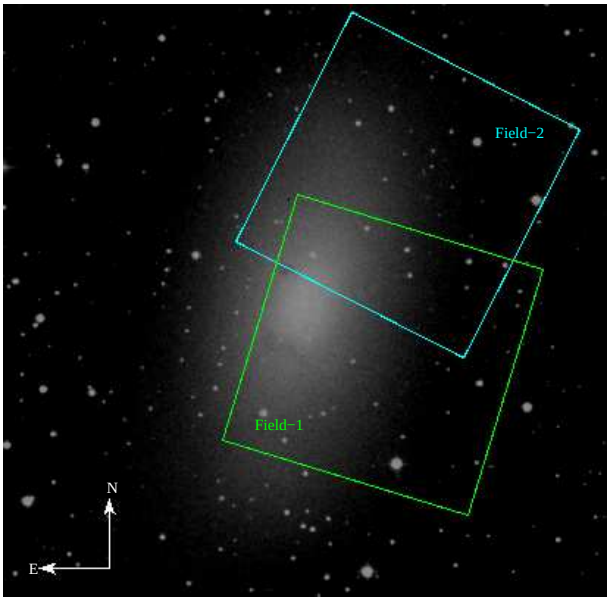

Figure 1. A 14.2×14.2 arcmin^2 POSSII image of NGC 205, retrieved from the NASA/IPAC Extragalactic Database. The two FoV (5.5×5.5 arcmin^2) we observed with GMOSGemini are superposed to the POSSII image.

The spectroscopic observations were obtained in queue mode with two gratings, R400+G5305 ('red') and B600 ('blue') during the nights of 8 and 10 October 2010. The effective 'blue' plus 'red' spectral coverage was generally from 3400 Å to 9600 Å, allowing an overlapping spectral range of about 300 Å. Exposure times were of 3×2,400 s per grating per field.

To avoid the possibility of having important emission-lines falling in the gap between the 3 CCDs, we slightly varied the central wavelength of the disperser from one exposure to another. So we centred R400+G5305 at 750 ±10 nm and B600 at 460 ±10 nm.

The slit width was 1″, while the slit heights varied from 5″ to 10″. Spatial pixels were binned. The final spatial scale and reciprocal dispersions of the spectra were as follows: 0.″161 and 0.09 nm per pixel, in 'blue'; and 0.″161 and 0.134 nm per pixel, in 'red'. The seeing varied from ∼0.42″ to ∼0.60″. CuAr lamp exposures were obtained with both gratings, in the day before or after the science exposures, following the usual procedure with Gemini+GMOS for wavelength calibration.

We performed observations of spectrophotometric standards (Massey et al. 1988; Massey & Gronwall 1990), with the same instrumental setups as for science exposures. BD284211 was observed with the red grating, on October 08, 2010, whereas Hiltner600 was the standard for the B600, ob-

Table 1. GMOS-N field identification, classification and coordinates of the [O III] line-emitters selected from the GMOS-N pre-imaging. F1(F2) stands for Field-1(Field-2). Our follow-up spectra give support to the object classification shown in the table.

Field-ID	Class	RA J2000.0	Dec J2000.0	C05/RM08
F1-1	star	00:39:57.93	41:40:51.06	-
F1-2	star	00:40:02.16	41:39:35.82	-
F1-3	star	00:40:06.07	41:37:54.33	-
F1-4	star	00:40:05.55	41:37:37.88	-
F1-6	star	00:40:05.17	41:39:27.32	-
F1-7	star	00:40:10.02	41:37:47.24	-
F1-8	PN	00:40:08.77	41:40:43.75	PN19/PN4
F1-9	PN	00:40:13.47	41:38:42.07	PN24/PN5
F1-10	PN	00:40:11.07	41:40:48.00	PN22
F1-11	star	00:40:11.37	41:37:48.58	-
F1-12	star	00:40:19.74	41:40:11.99	-
F1-13	PN	00:40:20.35	41:38:43.80	PN35
F1-14	PN	00:40:17.88	41:38:32.85	PN30/PN7
F1-15	PN	00:40:21.15	41:38:38.76	PN37
F1-16	PN	00:40:20.26	41:38:17.55	PN34/PN9
F1-18	-	00:40:20.88	41:41:42.10	PN36
F1-19	star	00:40:23.34	41:40:23.02	-
F1-20	PN	00:40:21.42	41:42:26.60	PN38/PN1
F1-21	PN	00:40:25.42	41:40:06.81	PN42
F1-22	PN	00:40:26.35	41:40:20.89	-
F2-1	star	00:40:04.35	41:40:33.21	-
F2-2	star	00:39:55.99	41:43:26.19	-
F2-3	PN	00:40:02.65	41:42:13.57	PN16/PN19
F2-4	PN	00:40:03.29	41:43:59.47	PN17/PN24
F2-5	star	00:40:06.38	41:44:55.35	-
F2-6	star	00:40:06.10	41:44:41.30	-
F2-7	PN	00:40:14.94	41:42:02.11	PN26
F2-8	-	00:40:07.97	41:45:23.64	PN18
F2-9	-	00:40:17.60	41:41:53.30	-
F2-10	PN	00:40:12.00	41:45:31.70	PN23
F2-11	PN	00:40:19.17	41:41:47.14	PN32
F2-13	star	00:40:15.72	41:47:06.28	-
F2-14	star	00:40:16.94	41:47:00.13	-
F2-15	PN	00:40:17.38	41:45:58.63	PN28

PN numbers given in column five correspond to the PN ID used by Corradi et al. (2005, C05) and Ciardullo et al. (1989), adopted by Richer & McCall (2008; RM08) in their spectroscopic study of part of Ciardullo's PN candidates. Sources F1-5, F1-17 and F2-12 where observed twice, so eliminated from this table and further analysis. Note that F1-18, F2-8 and F2-9 are actually symbiotic systems.

served on October 10, 2010. These frames were used to flux calibrate the spectra.

The observations were carried out at relatively low air-masses: typical airmass in 'blue' varied from 1.08 to 1.20; and in 'red' from 1.27 to 1.71, even though we attempt to align the slits to the parallactic angle (PA), so avoiding significant losses of light, especially in the blue end of the spectra, because of differential atmospheric refraction. Actually, the pre-imaging was carried out with fields positioned as we can see from Figure 1. Then the pre-images were rotated to build the masks for spectroscopy. For the blue exposure, during the observing nights the difference between the PA and the sky position angle at the telescope varied from 0 to 85 degree, always with air-masses above 1.2. From the Atmospheric Differential Refraction page in the GMOS website `http://www.gemini.edu`, we derived that at that airmass there is no light loss for $0.42 < \lambda < 0.60\mu$m and a negligible light loss ($\leqslant$20%) at $\lambda < 0.42\mu$m for the highest difference between the PA and the sky-position angle. For the red exposures, the differences between the PA and the sky-position angle were ∼20 degree for F1 (airmass from 1.3 to 1.7), and from 25 to 65 degree for F2 (airmass from 1.4 to 1.7). Thus

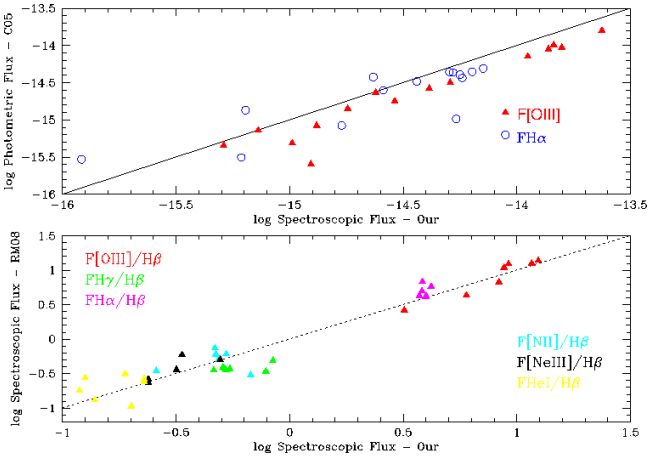

Figure 2. Comparison of the emission-line fluxes presented in Table A1 with the photometric fluxes of C05 (*top panel*) and the spectroscopic fluxes of RM08 (*bottom panel*). Lines of different wavelength and intensities are considered.

for F1, no light loss is expected, while for F2 we might have up to 40% of light loss for $\lambda > 0.8\mu$m. We double checked the three different exposures of F2 to see if significant amount of flux was lost in the red part of the spectra. Fortunately, the result is that the three exposure have similar number of counts, though they were taken over air-masses of 1.3, 1.5 and 1.7.

Data were reduced and calibrated in the standard way by using the Gemini GMOS DATA REDUCTION SCRIPT and LONG-SLIT tasks, both being part of IRAF[2]

3 RESULTS: THE SPECTROSCOPY OF PNE IN NGC 205

First, we use their spectroscopic features to classify the observed objects. As indicated in Table 1, out of the 37 slits we observed, 12 are stars; 3 are actually symbiotic systems, and all the others were confirmed as planetary nebulae. Some of these PNe are present in previous photometric catalogues (Corradi et al. 2005, hereafter C05) and spectroscopic studies (Richer & McCall 2008, hereafter RM08). Along the paper, we compare our observations to the results of C05 and RM08.

A few criteria were applied to distinguish the spectrum of a PN from possible mimics, as done in other works like Peña et al. (2007) and Magrini & Gonçalves (2009). (i) PNe were selected among point-like [O III]-emitting objects. Considering NGC 205 distance (0.77 Mpc; Howley et el. 2008), 1 arcsec corresponds to about 3.8 pc. Given the full width at half-maximum of about 0.6 arcsec for point-like objects, PNe (which have typically diameters smaller than 1 pc) are expected to be unresolved. (ii) Our PNe show faint or no continuum emission. The central stars ionising PNe are usually very hot (e.g. Stasińska 1990; Méndez, Kudritzki & Her-

[2] IRAF is distributed by the National Optical Astronomy Observatory, which is operated by the Association of Universities for Research in Astronomy (AURA) under cooperative agreement with the National Science Foundation.

rero 1992), much more than those of the H II regions. Due to their spectral type, with the energy maximum in the UV, PN central stars have lower M_V than the ionising stars of H II regions (typically more than 2 mag fainter). (iii) The presence of the He II 468.6nm emission (exceeding a few percent of Hβ) and/or [O III] 5007/H$\beta \geqslant 4$, define a spectrum as that of a PN of high-excitation. On the other hand, low-excitation PNe cannot be distinguished from compact H II regions only on the basis of their spectroscopic line ratios.

The emission-line fluxes were measured with the package SPLOT of IRAF. Errors on the fluxes were calculated taking into account the statistical errors in the measurement of the fluxes, as well as systematic errors (flux calibrations, background determination and sky subtraction). The observed line fluxes were corrected for the effect of the interstellar extinction using the extinction law of Mathis (1990) with R V = 3.1. We used c_β as a measurement of the extinction, which is defined as the logarithmic difference between the observed and theoretical Hβ fluxes. Since Hδ and Hγ are only available in few cases and are affected by larger uncertainties, c_β was determined comparing the observed Balmer I(Hα)/I(Hβ) ratio with its theoretical value, 2.85 (Osterbrock & Ferland 2006). Tables A1, in the Appendix section, gives the results of the emission-line flux measurements and extinction corrected intensities for all of PNe quoted as "PN" in the second column of Table 1. The ID of the photometrically identified PN candidates listed by C05 as well as those whose spectroscopic analysis were presented by RM08, are also given. Note that all the PNe studied in these two papers, located within the FoV of Figure 1, were recovered by the GMOS imaging, though, because of the limited number of slits we can observe simultaneously, we took spectra of only 7 of the RM08 PNe. F1-18, F2-8 and F2-9 will not be further discussed here, but separately in a forthcoming paper, since, their spectrum show that they are actually symbiotic systems, instead of PNe. In the optical (Belczyński et al. 2000), the spectra of symbiotics are indeed notable due to the absorption features and continuum of late-type M giants, the strong nebular emission lines of Balmer H I, He II and the forbidden lines of low- and high-ionization, like [O II], [Ne III], etc, or those of ions with an ionization potential of at least 35 eV (e.g. [O III]). Another conspicuous discriminator of symbiotic systems is the presence of the Raman scattered line at λ6830Å, a unique signature seen only in symbiotic stars (Schmid 1989, Belczyński et al. 2000).

In Figure 2 we contrast the observed emission-line fluxes presented in Table A1 with those given either from the spectroscopic data of RM08 or the photometric one of C05, for the objects in common. Note that we find a reasonable agreement for all the fluxes, no matter if photometric or spectroscopic, for a number of lines in a range of intensities and optical wavelengths.

In Table 2 we show our spectroscopic results, in terms of electron densities and temperatures, as well as ionic and total abundances of He, O, N, Ne, Ar and S, for all the PNe for which these information could be extracted, i.e., a total of 14 PNe.

As said before, there are 7 PNe of our sample that were already studied by RM08 (namely, in their work, as: PN1, 4, 5, 7, 9, 19 and 24). From these PNe we derived c_β, physical and chemical parameters for 6. We present in Table 3 a compilation of RM08 results, in order to make easier the comparison of ours and their figures.

Considering the c_β we give in Table A1, we get a mean value of 0.38±0.09 (not taking into account the null cases). This mean is slightly lower than that obtained from RM08 data (0.61; the average of the c_β(0.4 R_β E(B-V), R_β=3.041 was adopted in their paper). In Table 3 only 4 objects had the c_β determined using the same Balmer ratio as in our analysis. And, with the exception of PN9, the three other c_β values agree well. So, our c_β reasonably resembles theirs, though with a trend of being slightly lower. All in all, the PNe of NGC 205 have quite low extinction corrections, sometimes even as low as null, and never higher than 0.94 (PN9, RM08).

From Table 3 we promptly note that RM08 actually did not derive the electron densities for their PNe, instead they adopted a fixed values of 2,000 cm^{-3} to all of them. We, on the other hand, actually measured the ratio 6717Å/6737Å thus, we were able to derive the N_e[S II] for most of the PNe (see Table 2). We emphasise that here, for the first time, the electron density of the PNe of NGC 205 are obtained, though not for all PNe. As a matter of fact, with only one exception, none of these PNe has a N_e as low as the assumed value above, their mean value, with variance, being 5,300±860 cm^{-3}.

If electron temperatures are concerned, from our optical data it was possible to extract the T_e based on the [O III][(4959Å+5007Å)/4363Å] and on the [N II][(6548Å+6583Å)/5755Å] line ratios (for a number cases) and on one of these ratios ([O III]) for the rest of the sample. As it can be seen in Table 2, there is a good agreement between the two estimations of T_e, if errors, instead of only the face values, are considered. Moreover, T_e[N II]/T_e[O III] varying from 0.7 to 1.1 is expected, since they prove material at different regions of the nebulae and different excitation, as shown by Kaler (1986) and Krabbe & Copetti (2005). On average, T_e[O III] of our sample amounts to 13,250±3,150 K while for T_e[N II] the average value is 12,600±4,200 K. Now, by taking a look at the comparison in Table 3, what we get is that T_e[O III] is slightly higher in our analysis than in RM08, and we do not quite know why. However, if instead of considering only the PNe we have in common with RM08 we look at their whole sample (their Table 6), the average of their T_e[O III](variance) is 13,570(±2,350 K) (this average value is computed avoiding the PNe for which RM08 show upper limits), which is strictly in agreement with the average value we got from our own data.

Finally we come to the chemical abundances of Table 2. The details of the method we use for the derivation of abundances are exactly the same we applied in our previous studies, like for instance in Magrini & Gonçalves (2009) and Gonçalves et al. (2012). In short, the IONIC task of IRAF[3]. is combined with the ionisation correction factors from Kingsburgh & Barlow (1994) for the ionic and total abundances, respectively. In addition, when available, T_e[N II] is used for the calculation of the N^+, O^+, S^+ abundances, while T_e[O III] was used for the abundances of O^{+2}, S^{+2}, Ar^{+2}, He^+ and He^{+2}. In the remaining objects, where only

[3] The atomic data source is the that of ANALYSIS/NEBULAR – IRAF; http://stsdas.stsci.edu/cgi-bin/gethelp.cgi?at_data.hlp

Table 2. Electron temperatures, electron densities, ionic and total abundance of the PNe.

Diagnostic	F1-8	F1-9	F1-10	F1-13	F1-14	F1-15	F1-16	F1-20
T_e[O III](K)	18450±400	13800±240	12850±5450	13700±2300	12350±350	10650±950	12550±350	16000±2500
T_e[N II](K)	19000±1500	11100±2100			8400±2150	9850±350	10700±580	
N_e [S II](cm^{-3})	6600±50	4350±30			5750±60	7400±200	6300±60	3150±200
He I/H	0.091	0.076	0.084	0.081	0.084	0.099	0.084	0.080
He II/H	0.015	0.006	-	-	-	-	-	-
He/H	0.106±8.83e-04	0.082±5.93e-04	0.084±7.59e-03	0.081±2.55e-03	0.084±0.001	0.099±3.67e-3	0.084±1.01e-3	0.080±05.77e-3
O I/H	-	-	-	-	-	-	-	-
O II/H	5.026e-06	2.511e-05	8.350e-05	3.119e-06	6.264e-05	1.441e-04	6.588e-05	8.843e-06
O III/H	7.295e-05	1.577e-04	1.195e-04	8.570e-05	1.600e-04	8.807e-05	1.440e-04	1.802e-05
ICF(O)	1.103	1.053	1.000	1.000	1.000	1.000	1.000	1.000
O/H	8.606e-05	1.925e-04	1.195e-04	8.881e-05	2.226e-04	2.322e-04	2.099e-04	2.686e-05
12+log(O/H)	7.935±0.02	8.284±0.10	8.077±0.74	7.948±0.204	8.348±0.170	8.366±0.105	8.322±0.066	7.429±0.205
N II/H	1.907e-06	6.388e-06	-	5.887e-07	6.349e-06	1.780e-05	6.225e-06	2.276e-06
ICF(N)	13.945	2.946	-	21.359	-	1.688	2.710	2.508
N/H	3.266e-05	4.895e-05	-	1.677e-05	2.256e-05	2.868e-05	1.983e-05	6.914e-06
12+log(N/H)	7.514±0.20	7.690±0.19	-	7.224±0.116	7.353±0.519	7.458±0.043	7.297±0.037	6.840±0.101
Ne III/H	8.90e-06	1.960e-05	-	8.250e-06	1.740e-05	3.640e-06	1.830e-05	6.760e-06
ICF(Ne)	1.199	1.638	-	1.049	-	2.454	1.585	1.663
Ne/H	1.050e-05	2.391e-05	-	8.550e-06	2.421e-05	9.597e-06	2.667e-05	1.008e-05
12+log(Ne/H)	7.021±0.006	7.379±0.08	-	6.932±0.003	7.384±.136	6.982±0.023	7.426±0.032	7.003±0.037
Ar III/H	4.210e-07	-	4.900e-07	4.390e-07	7.140e-07	9.020e-07	8.530e-07	5.530e-07
Ar IV/H	-	-	-	-	-	-	-	-
ICF(Ar)	1.870	-	1.870	1.870	1.870	1.870	1.870	1.870
Ar/H	7.873e-07	-	9.163e-07	8.209e-07	1.335e-06	1.687e-06	1.595e-06	1.034e-06
12+log(Ar/H)	5.896±0.37	-	5.962e+00±0.50	5.914±0.116	6.126±0.519	6.227±0.043	6.203±0.037	6.015±0.101
S II/H	6.130e-08	2.555e-07	-	-	4.015e-07	2.517e-07	2.187e-07	4.678e-08
S III/H	1.210e-06	-	-	1.120e-06	-	-	-	2.978e-07
ICF(S)	1.710	1.120	-	1.954	-	1.024	1.101	1.085
S/H	2.217e-06	1.577e-06	-	2.399e-06	5.441e-06	6.196e-06	5.317e-06	3.884e-07
12+log(S/H)	6.365±0.027	6.198±0.10	-	6.380±0.032	6.736±0.379	6.792±0.001	6.726±0.015	5.589±0.056

Table 2 – *continued*

Diagnostic	F1-21	F2-4	F2-7	F2-10	F2-11	F2-15
T_e[O III](K)	12750±1300	8600±880	20650±1700	13900±1350	12250±650	11100±650
T_e[N II](K)	-	10850±2450	-	-	-	-
N_e [S II](cm^{-3})	6350±200	2650±0	-	750±30	-	-
He I/H	0.097	0.145	-	0.073	0.093	0.083
He II/H	0.004	-	0.062	-	-	-
He/H	0.101±4.32e-3	0.145±5.42e-3	0.062±8.36e-5	0.073±1.26e-3	0.093±9.89e-4	0.083±9.00e-4
O I/H	-	-	-	-	-	-
O II/H	1.792e-05	9.136e-05	-	3.762e-05	-	1.650e-06
O III/H	8.869e-05	2.137e-04	6.875e-05	2.819e-05	9.420e-05	2.057e-04
ICF(O)	1.030	1.000	1.000	1.000	1.000	1.000
O/H	1.097e-04	3.050e-04	6.875e-05	6.581e-05	9.420e-05	2.073e-04
12+log(O/H)	8.040±0.142	8.484±0.317	7.837±0.072	7.818±0.157	7.974±0.069	8.317±0.078
N II/H	3.093e-06	1.274e-05	8.115e-07	4.183e-06	4.190e-07	1.240e-06
ICF(N)	5.111	1.751	-	1.611	-	119.458
N/H	1.894e-05	4.253e-05	-	7.317e-06	-	1.344e-04
12+log(N/H)	7.277±0.068	7.629±0.162	-	6.864±0.071	-	8.129e+00
Ne III/H	9.820e-06	2.250e-05	8.280e-06	-	-	2.440e-05
ICF(Ne)	1.290	2.331	1.000	-	-	1.008
Ne/H	1.215e-05	3.212e-05	8.280e-06	-	-	2.460e-05
12+log(Ne/H)	7.085±0.014	7.507±0.139	6.918±0.082	-	-	7.391±0.001
Ar III/H	5.470e-07	1.500e-06	-	2.280e-07	6.350e-07	6.670e-07
Ar IV/H	-	-	-	-	-	-
ICF(Ar)	1.870	1.870	-	1.870	1.870	1.870
Ar/H	1.023e-06	2.805e-06	-	4.264e-07	1.187e-06	1.247e-06
12+log(Ar/H)	6.010±0.068	6.448±0.162	-	5.63±0.071	6.075±0.031	6.096±0.037
S II/H	9.936e-08	1.698e-07	-	4.270e-08	-	-
S III/H	-	8.810e-06	-	2.140e-06	3.410e-06	1.000e-06
ICF(S)	1.278	1.028	-	1.019	-	3.424
S/H	2.360e-06	1.033e-05	-	2.243e-06	-	3.482e-06
12+log(S/H)	6.373±0.019	7.014±0.050	-	6.351±0.003	-	6.542±0.006

T_e[O III] was measured, we adopted it both for low- and high-ionisation species. The abundances of He I and He II were computed using the equations of Benjamin, Skillman & Smits (1999) in two density regimes, that is $N_e > 1{,}000$ and $\leqslant 1{,}000$ cm^{-3}. The Clegg's collisional populations were taken into account (Clegg 1987).

We discuss the figures that come up from our abundance analysis in the following sub-section –abundance patterns–, here we simply compare our average abundances with those of RM08. First, as a consequence of the significant discrepancies between our and their electron temperatures, we also find a significant discrepancy when comparing both abundance, if only the PNe in common are considered. This is so because the temperature of the gas is a strong contributor in the derivation of the ionic abundances (see, Osterbrock & Ferland 2006). If, on the other hand, we take the average values of all PNe in RM08's Table 6 and our complete sample, both chemistries compare much better, in the last row of Table 3.

3.1 Abundance patterns

Considering that we want to use the chemical compositions of the PNe to study the luminosity(mass)-metallicity relations of the LG dwarf galaxies of different types, the dIrrs and dSphs, we need to check if O/H we derived above is or not a robust diagnostic of the ISM abundances at the time the progenitor stars at the center of these PNe were born. Though this is a phenomenon more relevant at very low metallicities (Péquignot et al. 2000; Leisy & Dennefeld 2006; Richer & McCall 2007; Magrini & Gonçalves 2009) type I PNe of the low-metallicity dwarf galaxies can produce and dredge-up oxygen to the surface of the central star, so to the nebular gas. The O/H of these type of PNe are of course not a good indicator of the ISM metallicity at

Table 3. c_β, electron temperatures, electron densities and total abundances of RM08, as compared to ours, the latter between brackets.

PN ID	c_β	T_e[O III] (K)	N_e [S II] (cm^{-3})	He/H	O/H[a]	N/H[a]	Ne/H[a]
PN1	- (0.53)	11,500(16,000)	2,000[c](3,150)	0.131(0.080)	8.21(7.42)	7.47(6.84)	7.48(7.00)
PN4	0.45(0.46)	15,100(18,450)	2,000[c](6,600)	0.122(0.106)	8.12(7.93)	8.17(7.51)	7.15(7.02)
PN5	0.42(0.36)	11,100(13,800)	2,000[c](4,350)	0.097(0.082)	8.53(8.28)	8.34(7.69)	7.71(7.37)
PN7	0.60(0.40)	11,900(12,350)	2,000[c](5,750)	0.121(0.084)	8.30(8.34)	7.87(7.35)	7.37(7.38)
PN9	0.94(0.41)	<15,200(12,550)	2,000[c](6,300)	0.103(0.084)	8.11(8.32)	7.20(7.29)	7.58(7.42)
PN24	- (0.12)	<16,200(8,600)	2,000[c](2,650)	0.066(0.145)	7.55(8.48)	- (7.62)	- (7.50)
Mean[b]	0.61(0.38)	13,570(13,250)	2,000[c](5,300)	0.108(0.090)	8.02(8.12)	7.38(7.39)	7.33(7.22)

[a] Abundances of O, N and Ne are given in units of 12 + log(X/H).
[b] The mean values are based on all the PNe described in Table 6 of RM08 and in our Table 2.
[c] RM08 electron densities (2,000 cm^{-3}) are assumed, instead of observed, values.

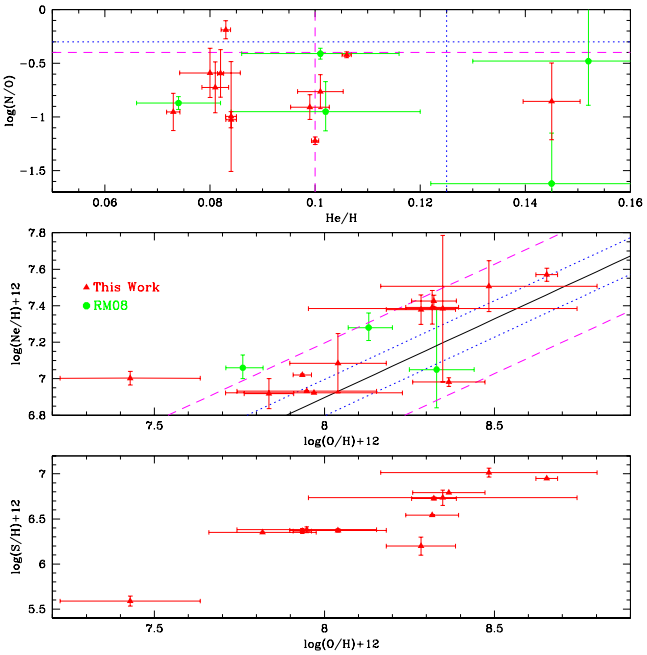

Figure 3. Various abundance patterns. *Top*: Log N/O vs. He/H for the brightest PNe of our sample (red triangles). RM08 PNe, which were not observed in the present work (see their Table 6), are represented in these plots as well (green circles). He/H$\geqslant$0.125 and log(N/O)$\geqslant$-0.3 give the region of the type I PNe, as defined from PNe of the Galaxy Perinotto et al. (2004), marked with short dashed lines. The limits for the SMC type I PNe Leisy & Dennefeld (2006) are marked with long dashed lines. In any case type I should populate the top right portion of the plot. *Middle*: Ne/H vs. O/H as compared the "universal" relationship between these two abundance ratios. The solid line is the fit for the PNe in the sample of Henry (1989). The dotted lines are placed at $\pm1\sigma$ and the dashed lines at $\pm3\sigma$, where σ=0.1dex. *Bottom*: S/H vs. O/H. Another α element, which should follow a similar relationship with oxygen as that of neon, since, as much as Ne, sulphur and oxygen have common origin.

the time progenitors were born. The latter happening, the PN abundances should be used with special care in analysis such as the forthcoming ones.

In Figure 3 we show some abundance patterns, including the log(N/O) versus He/H plot, in order to verify whether or not the PNe in our sample are significantly enriched in He and N. Following the definition based on Galactic PNe by Peimbert & Torres-Peimbert (1983), Kingsburgh & Barlow (1994), and others, type I PNe are nitrogen- and helium-enriched, with progenitors having likely undergone the third dredge-up and hot bottom-burning, and thus are likely to have higher progenitor masses (Peimbert & Torres-Peimbert 1983; Marigo 2001). By this criterion, type I PNe are located in this plot where He/H $\geqslant$ 0.125 and log (N/O) $\geqslant$ 0.3 (short-dashed lines) are defined for the Milky Way (see Perinotto, Morbidelli & Scatarzi 2004). However, because the metallicity of NGC 205 is similar to that of the Small Magellanic Cloud (SMC), we also include in this plot the equivalent criterion, defined by Leisy & Dennefeld (2006) using a large number of SMC PNe (long-dashed lines). The top-right portion of the plot, regardless of the criterion adopted, should be populated by the type I PNe of NGC 205. Clearly, from these criteria, there are no type I objects in our, or RM08, sample of PNe in NGC 205.

The other two panels of Figure 3 show the behaviour of the α elements (sulphur and neon) abundances as a function of the O/H. Neither Ne nor O are usually produced during the lifetime of the PN progenitors in significant amounts, and, in the case of NGC 205's PNe there is no reason to think differently. In fact, the abundances of these two elements seem to vary in lockstep, where the slope of the log-log relation is very close to unity (cf. Henry 1989), as we see in the middle panel of Figure 3. This behaviour is essentially the same for H II regions (Vigroux et al. 1987; Izotov et al. 2006) and it seems independent of the host galaxy. As shown by Henry (1989), by putting together the Ne and O abundances of 157 PNe, planetary nebulae of the Galaxy, LMC, SMC and M31 all follow the "universal" relation of Ne vs. O, with a slope of +1.16 in the log-log plot (continuous line plotted in the middle panel of the figure). S/H vs. O/H also follows a similar trend with oxygen as that of neon, since, sulphur and oxygen also have common origin. Note that RM08's PNe not re-observed in the present work follow the same behaviour of our own sample (green symbols). So, altogether, we can conclude that oxygen is a reliable tracer of the ISM composition at the time of the PN progenitor birth.

3.2 PN progenitors ages and masses

It is possible to estimate the central star luminosity and effective temperature (T_{eff}) by using our optical spectra. To understand the limits and the assumptions of these estimations, there are few considerations that need to be done. First, T_{eff} is obtained from the Zanstra temperature, using the formulae by Kaler & Jacoby (1989) when applied to extragalactic PNe (see Kniazev et al. 2005). These relations assume that the PNe are optically thick in the He-

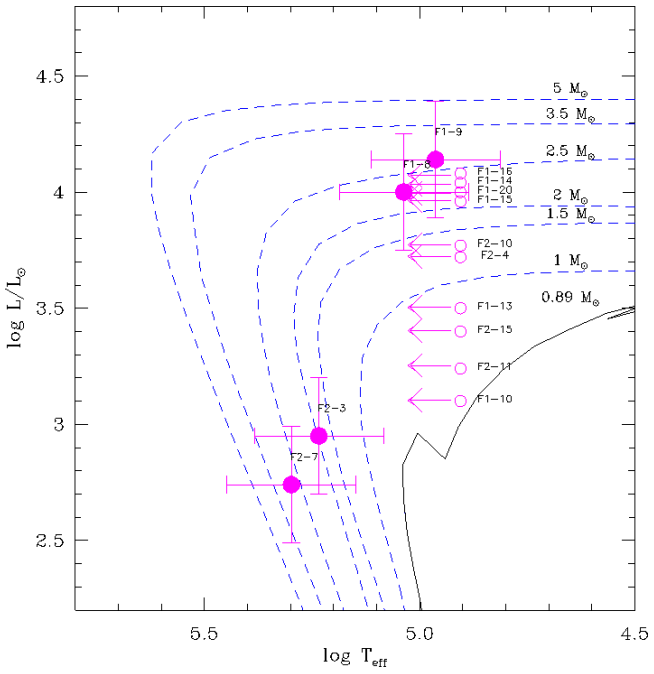

Figure 4. Vassiliadis & Woods (1994) tracks (z=0.004, dashed lines for H-, and continuous line for He-burning tracks), with superimposed the central stars' effective temperatures and luminosities, for the PNe for which we computed chemical abundances. The filled circles are PNe with He II detected, thus those for which the T_{eff} can be directly obtained. The empty circles are PNe without He II lines, so their T_{eff} is considered constant at 80,000 (which the value obtained in the Zanstra relationship if we consider He II λ4686=0).

ionising continuum. Thus, the derived T_{eff} is an upper limit when He II λ4686 is not detected, and a lower limit when He II λ4686 is detected and the nebula is optically-thin in the He-ionising continuum. Only in those cases when He II λ4686 is detected and the nebula is optically thick in the ionising continuum for He^+, so the Zanstra temperature fulfils the conditions for its derivation. For the total luminosities of the PN central stars, the relations given in Gathier & Pottasch (1989) and Zijlstra & Pottasch (1989) were applied, considering the photometric [O III] fluxes –that include both lines of the [O III] doublet– of C05, and scaling them with the ratio between Hβ and [O III], to obtain the photometric Hβ flux. We then corrected the Hβ fluxes for reddening, and adopted a distance of 770 kpc to NGC 205 to compute the absolute luminosities. We note that the so-computed stellar luminosities are upper limits in all cases when the nebula is optically-thin in the H-ionising continuum. Masses, on the other hand, were derived from to theoretical evolutionary tracks of Vassiliadis & Wood (1994) for Z = 0.004 (1/5 $Z_{\odot}$). Ages were estimated using the evolutionary lifetimes of the various phases of the progenitor stars, from Vassiliadis & Wood (1993). For the four PNe in which He II λ4686 was measured, we give an estimate of their luminosity and T_{eff}. For the remaining PNe, we give an upper limit of their T_{eff}, conservatively considering the flux of He II λ4686=0. There are two possibilities to understand their location in the HR diagram: either these stars have low temperatures, and they originate from very low mass progenitors –perhaps of unreasonably low mass–, or the detection limit for He II is such that their true temperatures may be higher, near logT_{eff}=5.2 dex, and thus they are consistent with the evolutionary track of $\sim$2$M_{\odot}$. Given the number of stars with these characteristics, the second possibility is the most probable one. Having in mind the limits in the above calculations, we conclude that the so-derived effective temperatures and luminosities of the central stars allow us to determine an upper limit to the mass distribution for the progenitor stars and the age for the youngest progenitors only, which are characterised by masses of $\sim$2-2.5 $M_{\odot}$, and thus were born between 1.0 and 1.7 Gyr ago.

4 THE LUMINOSITY- AND MASS-METALLICITY RELATIONS FOR THE LG DWARF GALAXIES

Given the history of the LZR –the controversial existence or not of an offset in the sense that for a given luminosity higher metallicities would be found for the dSphs as compared with the dIrrs–, we re-analyse the PN LZR and the MZR of the LG dwarfs, in Figure 5 and Figure 6.

4.1 The luminosity-metallicity relation

To build the LZR, the oxygen abundances of the PN population of the galaxies were found in our own previous studies, and in a number of others from the literature (see Fig. 5). Particularly in the case of NGC 205, the mean O/H was derived from the data in the present work, the 14 PNe in Table 2, plus the 7 PNe of RM08 not included in this paper. Thus, the 21 PNe give a 12+log(O/H) = 8.03$\pm$0.29. The luminosities (M_B) are from Mateo (1998), Lee et al. (2003) and van den Bergh (2007). The continuous line shown in Figure 5 gives the weighted least-squares fit to the metallicity versus luminosity data for the 50 dIrrs within a distance of 5 Mpc. This fit,

$$12 + log\ (\tfrac{O}{H}) = 5.67 - 0.151\ M_B, \quad (1)$$

was obtained from the galaxies' H II regions, as given in the compilation of van Zee et al. (2006). The first aspect to be noticed in Figure 5 is that the location of the dIrrs and dSphs in the LZR cannot be clearly separated from each other, meaning that the offset we found previously (see Fig. 6 of Gonçalves et al. 2007) has vanished. The latter is due to the fact that in the present version of the plot we use new measurements of PN metallicities (the O/H of PN population in M32, NGC 3109, NGC 6822, NGC 185, NGC 205 and SMC come from analysis published after 2007; see the caption of Fig. 5). Coherently, this is in agreement with the latest results from the spectroscopically determined stellar LZR (Kirby et al. 2013).

We note that only one dIrr (and none dSph) was added to the LZR since the analysis of 2007, namely IC 10 (Magrini & Gonçalves 2009). However, the O/H of several (M32, NGC 3109, NGC 6822, NGC 185, NGC 205 and SMC) dwarf galaxies had been revised, so, altogether 7 of the 14 objects in the plot had their O/H changed somewhat.

As a matter of fact, oxygen was produced, and brought to the surface of the central stars via the third dredge-up in a few PNe of the dIrrs Sex A (Magrini et al. 2005) and NGC 3109 (Peña et al. 2007). Judging from Figure 5, if these

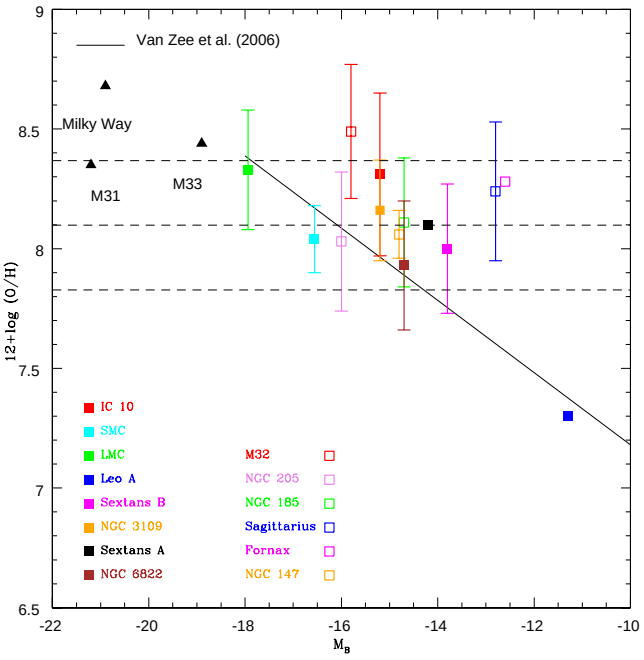

Figure 5. The PNe luminosity-metallicity relation of the LG dwarf galaxies, showing 12+log(O/H) vs. magnitude. Filled symbols represent the dIrrs while the dSphs are have empty symbols. The standard deviation of the abundances in a given galaxy is also plotted, except for the galaxies in which only one PN had its oxygen abundance determined. The continuous line represents the LZR, from H II regions of nearby (D $\leqslant$ 5 Mpc) galaxies with magnitudes fainter than -18 (van Zee et al., 2006). The dashed lines represent the mean value and standard deviation (8.098±0.27) for the PNe of all the dwarf galaxies in the plot. References for the 12+log(O/H) are: IC 10, Magrini & Gonçalves (2009); SMC, Shaw et al. (2010); LMC, Leisy & Dennefeld (2006); Sextans A and Sextans B, Magrini et al. (2005); Leo A, van Zee et al. (2006); NGC 3109, Peña et al. (2007); NGC 6822, Hernández-Martinez et al. (2009); M32, RM08; NGC 205, this work plus RM08; NGC 185, Gonçalves et al. (2012); Sagittarius, Zijlstra et al. (2006) and Otsuka et al. (2011); Fornax, Kniazev et al. (2007); and NGC 147, Gonçalves et al. (2007); M31, Jacoby & Ciardullo (1999), Kwitter at al. (2012), Balick et al. (2013); Milky Way, Perinotto et al. (2004); M33, Magrini et al. (2009). Luminosities (M_B) of the dwarf galaxies are from the Mateo (1998), with the exception of those for the LMC and SMC that are from Lee et al. (2003). M_B of the Galaxy, M31 and M33 are from van den Bergh (2007).

two galaxies were excluded, the LZR of the dIrrs would not change significantly. However, and fortunately, the phenomena of oxygen production in PNe is a rare one, and occurs mainly for 12+log(H/O)$\leqslant$7.7 (see Magrini & Gonçalves 2009 for a complete discussion on the third dredge-up of oxygen in the LG dwarfs). Following Kniazev et al. (2007), the self-production of oxygen occurred in the dSph Fornax. These authors propose to lower the 12+log(O/H) by 0.27±0.10 in order to reconcile the galaxy abundance patterns of S/O, Ne/O and Ar/O with the expected values. At variance with Sex A and NGC 3109, in the case of Fornax, such a correction would actually make it better correlate with the other dSphs of the LZR. However, the O/H for Fornax is based on only one PN, so probably neither representing the oxygen abundance in all of the stars in this galaxy, nor the stellar population to which its progenitor star belonged. It is worth mentioning as well that the enrichment in Sgr may have been accelerated by the lack of metal-poor gas (as compared to isolated dIrr galaxies), or by accretion of enriched gas expelled by our Galaxy, as pointed out in Zijlstra et al. (2006). A decrease of the O/H of Sgr would better locate this galaxy in the LZR defined by the remaining dSphs. Also, a higher luminosity for Sgr would make it better agrees with the location of the other data points in the relation, and, in all likelihood, its luminosity before its interaction with the Milky Way was substantially higher than that of Fornax.

4.2 The mass-metallicity relation

In addition to the LZR, we present in Figure 6 the mass-metallicity relation of the LG dwarf galaxies. The stellar masses of the LG galaxies were taken from the compilation by McConnachie (2012), while the oxygen abundances are from the analysis of PN spectra, as in Fig. 5. First, we note that, as in the case of the LZR, dIrrs and dSphs are not segregated, and follow a common relation.

In Figure 6 we plot the least-squares fit obtained by Kirby et al. (2013, see their eq. 4) using the stellar metallicities in dwarf galaxies and our least mean square fit. We added a constant to the Kirby's et al. (2013) interception of the Y-axis to match the nebular metallicity, expressed in our plot as 12 + log(O/H). The Kirby's relation becomes:

$$12 + log\ (\frac{O}{H}) = (-1.69 - 1.8 + A) + 0.3 \times log\ (\frac{M\star}{M_\odot}) \qquad (2)$$

where -1.69 is the original intercept from the fit of Kirby et al. (2013), obtained using log ($M\star \times 10^6 M_\odot$), −1.8 is the constant that takes into account that our abscissa is expressed in log($M\star/M_\odot$) and A=9.25 is the constant needed to match the data. The choice of A=9.25 dex translates the Kirby et al. (2013) relation to the region of Fig. 6 occupied by our data. While the slope is relevant for comparison with our data and the other relations in Fig. 6, the zero point is not. The least mean square fit to our data gives the following relation:

$$12 + log\ (\frac{O}{H}) = 6.19 + 0.24 \times log\ (\frac{M\star}{M_\odot}). \qquad (3)$$

The fit presented in Eq. 3 is very sensitive to the data points for the LMC and Leo A. However, excluding them would mean to limit the mass range from log($M\star/M_\odot$)$\sim$7.5 to 8.

The lowest mass in Kirby's et al (2013) was of the order of $10^3 M_\odot$. In Figure 6, we encompass a smaller stellar mass range ($10^7 M_\odot$ to $10^9 M_\odot$) in which we find that the MZR has a slope similar to that of the relation built with stellar metallicities. The MZR with oxygen abundances seems to deviate only when reaching the stellar mass of the dIrr Leo A with $M_\star < 10^7 M_\odot$.

In Figure 6, we also show the comparison with the mass-metallicity relation for $M_\star$ stacks, obtained with Sloan SDSS Data Release 7 by Andrews & Martini (2013). They measured [O III], [O II], [N II], and [S II] electron temperatures, and from them, they adopted the direct method gas-phase oxygen abundances from stacked galaxy spectra. They stacked the spectra of $\sim$200,000 SDSS star-forming galaxies in bins of 0.1 dex in stellar mass. Thus, the Andrews & Martini (2013)'s MZR is better comparable with our results

than MZR obtained with methods that do rely on strong line diagnostics (e.g. Tremonti et al. 2004).

Excluding Fornax and Sgr, discussed in the previous section, we note that the oxygen abundances of PNe trace the same metallicity as H II regions in the Sloan SDSS. In particular we do not see any offset from the average metallicity in each bin of stellar mass. We also note that the dIrr galaxy Leo A deviates from the linear fit, and it is located below both the Van Zee et al. (2006)'s fit of Fig. 5 and the Kirby et al. (2013)'s fit of Fig. 6. However, the location of Leo A is perfectly consistent with the extrapolation of the asymptotic logarithmic fit of the SLOAN mass-metallicity relation shown in Fig. 6. Note that this is among the metal poorest points added to the MZR relation built with oxygen abundances.

The results shown in Figure 6 points out a *possible* universality of the MZR for both dIrr and dSph galaxies. There is still a non-negligible scatter among the data points based upon the chemical composition from PNe. At variance with the previous results (see Richer & McCall 1995, Gonçalves et al. 2007), based on small statistics and non-homogeneous analysis and indicating a clearly different behaviour of dIrr and dSph galaxies, now these two classes of galaxies are compatible with a unique mass-metallicity relation. Being very conservative, we can conclude saying that at present neither the data nor the mass-metallicity relations are known well enough to *categorically* affirm that dwarf irregulars and dwarf spheroidals follow the same mass-metallicity relation, though they are now fully compatible with this possibility. This was not the case previously. It is interesting to notice that both dIrrs and dSphs are consistent with global MZR of star forming galaxies, likely because chemical evolution is a function of stellar mass and its correlation with the total mass (baryonic and non-baryonic) of the galaxy.

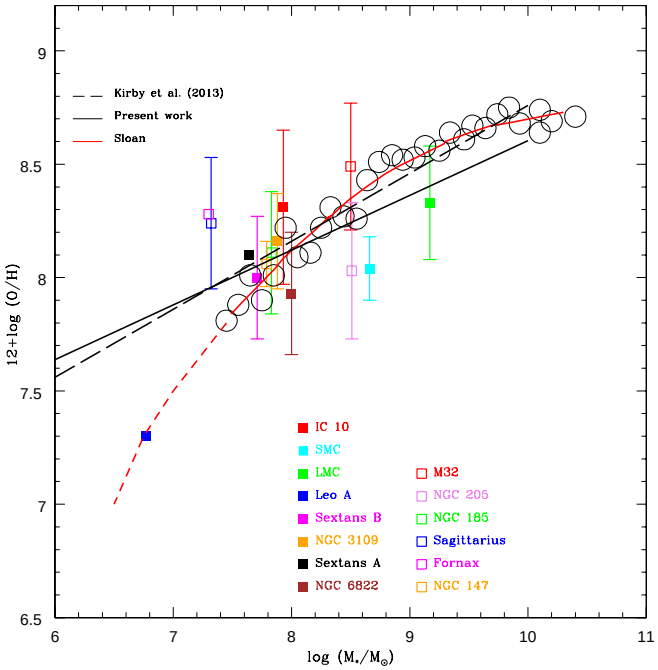

Figure 6. The PN mass-metallicity relation of the LG dwarf galaxies, showing 12+log(O/H) vs. stellar mass. Filled symbols represent the dIrrs while the dSphs are have empty symbols. The standard deviation of the abundances in a given galaxy is also plotted, except for the galaxies in which only one PN has its oxygen abundance determined. References for the 12+log(O/H) are the same as in Figure 5. Data for stellar masses were taken from the compilation by McConnachie (2012). The dashed line represents the mass-stellar metallicity relation of Kirby et al. (2013) to which we added a constant to match the oxygen metallicity, while the continuous line is the mean least square fit to our data. The direct method mass-metallicity relation for $M_\star$ stacks in Sloan SDSS Data Release 7 (DR7; Abazajian et al. 2009) (empty circles) from Andrews & Martini (2013). The red solid curve shows the asymptotic logarithmic fit to the direct method measurements. The dashed red curve is an extrapolation of the fit.

5 CONCLUSIONS

In this paper our new optical observations for NGC 205, obtained using the GMOS at Gemini, a multi object imager and spectrograph, were presented. By applying the narrow-band [O III] - $[O\ III]_{cont}$ technique, we identified a number of 37 PN candidates, which were then studied in terms of their physical and chemical properties. 16 of these candidates were actually confirmed to be PNe. Another three were identified as symbiotic systems (Gonçalves et al, in prep).

The analysis of the PN optical spectra allowed us to derive the electron densities (N_e; none of the NGC 205 PNe had its N_e determined previous to the present work), the electron temperatures (T_e) and ionic as well as total abundances. These PN properties were compared with the only good enough previous work about the spectroscopy of the PNe in NGC 205 (Richer & McCall 2008) and, in general, both analysis are in agreement.

The chemical patterns and evolutionary tracks derived for 14 of our PNe suggest that there are no type I planetary nebulae in the present sample, which also implies that the PN average oxygen abundance (12+log(O/H)=8.08±0.28) of NGC 205 is a robust diagnostic of the ISM metallicity by the time the progenitor stars were born, about 1.0 to 1.7 Gyr ago. Altogether NGC 205's PNe are relatively young (latter figures), as it is implied by the mass range of their progenitors, between 2 and 2.5 $M_\odot$.

We have been studying for years the metallicity trends of the LG dwarf galaxies, as seen from these galaxies PN population (Magrini et al. 2005, Leisy et al. 2005, 2006, Gonçalves et al. 2007, Magrini & Gonçalves 2009, Gonçalves et al. 2012), among others, with the goal to establish the PNe luminosity- and mass-metallicity relations for the nearby dIrrs as well as the dSphs. Previous attempts to obtain such relations have been shown to be based on a too limited sample and poorly measured abundances (Richer & McCall 1995; Gonçalves et al. 2007). We revisited this issue using more and more accurate data, and found results that contradict the previous ones, but that agree very closely with the new LZR and MZR obtained recently by using stellar metallicities (Kirby et al. 2013).

Using spectroscopic stellar metallicities for dIrrs and dSphs, Kirby et al. (2013) have recently shown that dwarf irregulars obey the same mass-metallicity relation as the dwarf spheroidals, and they also have shown this relationship is roughly continuous with the stellar mass-stellar metallicity relation for galaxies as massive as $M_* = 10^{12}$ $M_\odot$.

It is extremely interesting to note that, the slope of the MZR given by the PNe metallicities in the present work, is the same as that obtained by using stellar metallicities. The stellar masses of the galaxies in our sample correspond to 10^7 up to 10^9 $M_\odot$. On the other hand, in Kirby et al. (2013) galaxies of smaller stellar masses ($>10^3$ $M_\odot$) are also studied, and, in addition, using the H II region metallicities recently obtained for more massive galaxies (SDSS; Andrews & Martini (2013), the universality of the MZR is strongly reinforced by the present analysis.

And, a final aspect of the our results that it is worth highlighting is that not only the MZR for both dIrr and dSph galaxies are consistent with the same relation, at variance with the differences claimed in the past, but also the MZR of both dIrrs and dSphs are consistent with the global MZR of star-forming galaxies.

6 ACKNOWLEDGMENTS

Authors are very grateful with Anna Gallazzi and Evan Kirby for their critical reading of the manuscript and a number of fruitful discussions. We also thanks the careful report of the referee, Michael Richer, which helped us to significantly improve the paper. DRG kindly acknowledges the Instituto de Astrofísica de Canarias (IAC) for their hospitality, where part of this work was done. CMC is supported by CAPES. This work was also partially supported by FAPERJ's grant E-26/111.817/2012. LM acknowledge financial support from PRIN MIUR 2010-2011, project "The Chemical and Dynamical Evolution of the Milky Way and Local Group Galaxies", prot. 2010LY5N2T.

REFERENCES

Abazajian K. N., Adelman-McCarthy J. K., Agüeros M. A., Allam S. S., & Allende-Prieto C., et al., 2009, ApJS, 182, 543
Andrews B. H., & Martini P., 2013, ApJ 765, 140
Baade W., 1944, ApJ, 100, 137
Balick B., Kwitter K. B., Corradi R. L. M., Henry R. B. C., 2013, ApJ, 774, 3
Belczyński K., Mikołajewska J., Munari U., Ivison R. J., & FriedjungX M., 2000, A&AS, 146, 407
Benjamin R. A., Skillman E. D., Smits D. P., 1999, ApJ, 514, 307
Bertola F., Bressan A., Burstein D., Buson L. M., Chiosi C., di Serego Alighieri S., 1995, ApJ, 438, 680
Bica E., Alloin D., Schmidt A. A., 1990, A&A, 228, 23
Cappellari M., Bertola F., Burstein D., Buson L. M., Greggio L., Renzini A., 1999, ApJ, 515, L17
Cepa J., Beckman J. E., 1988, A&A, 200, 21
Ciardullo R., Jacoby G. H., Ford H., & Neill J.D., 1989, ApJ, 339, 53
Clegg R. E. S., 1987, MNRAS, 229, 31
Corradi R. L. M., et al., 2005, A&A, 431, 555
Davidge T. J., 2003, ApJ, 597, 289
De Looze I., et al., 2012, MNRAS, 423, 2359
Ford H. C., Jacoby G., & Jenner D. C., 1977, ApJ, 213, 18
Gathier R., Pottasch S. R., 1989, A&A, 209, 369
Gilmore G., Wyse R. F., 1991, ApJ, 367, L55
Gonçalves D. R., Magrini L., Leisy P., Corradi R. L. M., 2007, MNRAS, 375, 715
Gonçalves D. R., Magrini L., Martins L. P., Teodorescu A. M., Quireza C., 2012, MNRAS, 419, 854
Grebel E. K., Gallagher J. S., III, & Harbeck D., 2003, AJ, 125, 1926
Grebel E. K., 2005, in Mikolajewska J., Olech A., eds, AIP Conf. Proc. 752, Stellar Astrophysics with the Worlds Largest Telescopes: First International Workshop on Stellar Astrophysics with the Worlds Largest Telescopes. American Institute of Physics, New York, p. 161
Hernández-Martínez L., Peña M., Carigi L., & García-Rojas J., 2009, A&A, 505, 1027
Henry R. B. C., 1989, MNRAS, 241, 453
Hodge P. W., 1973, ApJ, 182, 671
Howley K. M., Geha M., Guhathakurta P., Montgomery R. M., Laughlin G., & Johnston K. V., 2008, ApJ, 683, 722
Izotov Y. I., Stasińska G., Meynet G., Guseva N. G., & Thuan T. X., 2006, A&A, 448, 955
Jacoby G. H., & Ciardullo R., 1999, ApJ, 515, 169
Kaler J. B., 1986, ApJ, 308, 322
Kaler J. B., Jacoby G. H., 1989, ApJ, 345, 871
Kingsburgh R. L. & Barlow M. J., 1994, MNRAS, 271, 257
Kirby E. N., Cohen J. G., Guhathakurta P., Cheng L., Bullock J. S., Gallazzi A., 2013, ApJ, 779, 102
Kniazev A. Y., Grebel E. K., Pustilnik S. A., Pramskij A. G., & Zucker D. B., 2005, AJ, 130, 1558
Kniazev A. Y., Grebel E. K., Pustilnik S. A., & Pramskij A. G., 2007, A&A, 468, 121
Koleva M., Bouchard A., Prugniel P., De Rijcke S., & Vauglin I., 2013, MNRAS, 428, 2949
Kormendy J, Djorgovski S., 1989, ARA&A, 27, 235
Krabbe A. C. & Copetti M. V. F., 2005, A&A, 443, 981
Kwitter K. B., Lehman E. M. M., Balick B., & Henry R. B. C., 2012, ApJ, 753, 12
Lee H., McCall M. L., Kingsburgh R. L., Ross R., Stevenson C. C., 2003, AJ, 125, 146
Lee H., Bell E. F., & Somerville R. S., 2008, in IAU Symp. 255, Low- Metallicity Star Formation: From the First Stars to Dwarf Galaxies, ed. L. K. Hunt, S. Madden, & R. Schneider (Cambridge: Cambridge Univ. Press), 100
Leisy P., Dennefeld M., 2006, A&A, 456, 451
Leisy P., Magrini L., Corradi R., Mampaso A., 2005, AIPC, 804, 265
Leisy P., Magrini L., Corradi R. L. M., Mampaso A., 2006, pnbm.conf, 252
Lianou S., Grebel E. K., & Koch A., 2011, A&A, 531, 152
Magrini L., Leisy P., Corradi R. L. M., Perinotto M., Mampaso A., Vilchez J. M., 2005, A&A, 443, 115
Magrini L., Gonçalves D. R., 2009, MNRAS, 398, 280
Magrini L., Stanghellini L., & Villaver E., 2009, ApJ, 696, 729
Marigo P., 2001, A&A, 370, 194
Massey P., Strobel K., Barnes J. V., Anderson E., 1988, ApJ, 328, 315
Massey P., Gronwall C., 1990, ApJ, 358, 344
Mateo M. L., 1998, ARA&A, 36, 435
Mathis J. S., 1990, ARA&A, 28, 37
McConnachie A. W., 2012, AJ, 144, 4
Méndez R. H., Kudritzki R. P., & Herrero A., 1992, A&A, 260, 329

Monaco L., Saviane I., Perina S., Bellazzini M., Buzzoni A., Federici L., Fusi Pecci F., Galleti S., 2009, A&A, 502, L9
Osterbrock D. E. & Ferland G. J., in Astrophysics of gaseous nebulae and active galactic nuclei, 2nd. ed. Sausalito, CA: University Science Books, 2006
Otsuka M., Meixner M., Riebel D., Hyung S., Tajitsu A., Izumiura H., 2011, ApJ, 729, 39
Peimbert M., Torres-Peimbert S., 1983, in Flower D. R., Proc. IAU Vol. 103, Planetary Nebulae. Reidel, Dordrecht, p. 233
Peña M., Stasińska G., & Richer M. G., 2007, A&A, 476, 745
Perinotto M., Morbidelli L., Scatarzi A., 2004, MNRAS, 349, 793
Péquignot D., Walsh J. R., Zijlstra A. A., & Dudziak G., 2000, A&A, 361, L1
Richer M. G., McCall M. L., 1995, ApJ, 445, 642
Richer M. G., McCall M. L., 2007, ApJ, 658,328
Richer M. G., McCall M. L., 2008, ApJ, 684, 119
Salaris M., & Girardi L., 2005, MNRAS, 357, 669
Saviane I., Held E. V., & Bertelli G., 2000, A&A, 355, 56
Shaw R. A., Lee T.-H., Stanghellini L., Davies J. E., García-Hernández D. A., et al., 2010, ApJ, 717, 562
Stasińska G., 1990, A&AS, 83, 501
Skillman E. D., Kennicutt R. C., Hodge P. W., 1989, ApJ, 347, 875
Tremonti C. A., Heckman T. M., Kauffmann G., Brinchmann J., Charlot S., et al., 2004, ApJ, 613, 898
van den Bergh S., 2007, in The Galaxies of the Local Group, Cambridge: Cambridge University Press, 2007
van Zee L., Skillman E D., & Haynes M. P., 2006, ApJ, 637, 269
Vassiliadis E., Wood P. R., 1993, ApJ, 413, 641
Vassiliadis E., Wood P. R., 1994, ApJS, 92, 125
Vigroux L., Stasińska G., & Comte G., 1987, A&A, 172, 15
Young L. M., Lo K. Y., 1997, ApJ, 476, 127
Zijlstra A. A., Pottasch S. R., 1989, A&A, 216, 245
Zijlstra A. A., Gesicki K., Walsh J. R., Péquignot D., van Hoof P. A. M., & Minniti D., 2006, MNRAS, 369, 875

APPENDIX A: EMISSION-LINE FLUX MEASUREMENTS

In this section we present the observed emission-line fluxes and extinction corrected intensities measured in our sample of PNe.

Table A1. Observed fluxes and extinction corrected intensities of our PNe. Column (1) gives the PN name; column (2) gives the observed Hβ flux in units of 10^{-16} erg cm^{-2} s^{-1}; column (3) the nebular extinction coefficient; columns (4) and (5) indicate the emitting ion and the rest frame wavelength in Å; columns (6), (7), and (8) give extinction corrected (I_λ) intensities, the relative error on the fluxes (ΔF_λ) and the measured fluxes (F_λ). Both I_λ and F_λ are normalised to Hβ=100. Upper limits on the line fluxes are marked with :.

Id	$F_{H\beta}$	c_β Δc_β	Ion	λ (Å)	I_λ	ΔF_λ (%)	F_λ
F1-8	13.58	0.458 ±0.005	He I	3734	1.4	0.9	1.0
			He I	3872	61.8	1.7	47.7
			H I	3889	14.2	1.1	11.0
			[Ne III]	3968	40.1	1.5	31.8
			He I	4026	4.6	0.3	3.7
			Hδ	4100	27.0	0.9	22.1
			Hγ	4340	59.2	1.1	51.7
			[O III]	4363	32.7	1.0	28.7
			He I	4471	7.4	0.8	6.7
			He II	4547	1.2	0.5	1.1
			He II	4686	13.5	0.6	12.9
			Ar IV	4712	3.7	0.3	3.6
			Ar IV	4740	5.9	0.4	5.8
			Hβ	4861	100.0	0.8	100.0
			He I	4922	1.3	0.3	1.3
			[O III]	4959	376.3	1.7	386.1
			[O III]	5007	1120.7	2.7	1164.2
			He I	5016	3.5	0.3	3.6
			[Fe III]	5085	0.5	0.1	0.5
			[Fe II]	5159	0.3	0.2	0.3
			[N I]	5200	0.7	0.2	0.7
			[Fe III]	5412	0.9	0.1	1.1
			C IV	5802	0.5	0.1	0.6
			[O I]	5577	11.4	0.3	13.5
			[Fe II]	5582	18.1	0.2	21.6
			[N II]	5755	1.8	0.2	2.2
			He I	5876	18.4	0.3	22.9
			[Si II]	6347	0.4	0.2	0.5
			O I	6363	1.4	0.2	1.8
			[N II]	6548	12.0	0.3	16.5
			Hα	6563	289.9	1.0	399.2
			[N II]	6584	35.4	0.4	48.9
			He I	6678	4.5	0.3	6.3
			[S II]	6717	1.5	0.2	2.2
			[S II]	6731	2.7	0.2	3.8
			[Ar V]	7006	1.4	0.1	2.0
			He I	7065	13.7	0.1	20.3
			[Ar III]	7135	14.6	0.1	21.9
			[O II]	7320	6.6	0.2	10.1
			[O II]	7330	5.9	0.2	9.1
			[Ar III]	7751	3.0	0.1	4.9
			H I	8665	0.8	0.1	1.6
			H I	8750	1.4	0.2	2.7
			H I	8862	2.4	0.1	4.5
			H I	9015	1.4	0.2	2.7
			[S III]	9069	13.3	0.3	26.5
			H I	9229	2.0	0.3	4.0
			He I	9526	46.9	0.3	100.1
			H I	9546	3.0	0.1	6.4
F1-9	19.05	0.366 ±0.003	He I	3587	14.6	0.9	11.2
			H I	3667	3.6	0.7	2.8
			[O II]	3726	18.2	1.2	14.4
			H I	3771	2.1	0.8	1.7
			H I	3798	2.5	0.9	2.0
			[Ne III]	3868	60.9	1.4	49.5
			H I	3889	11.4	1.0	9.3
			He II	3922	2.3	1.0	1.9
			[Ne III]	3968	39.2	1.1	32.5
			[F IV]	4060	2.9	0.9	2.5
			[Si II]	4069	4.8	0.9	4.1
			Hδ	4100	31.0	1.0	26.5
			Hγ	4340	56.7	1.1	50.9
			[O III]	4363	19.1	0.7	17.2
			O II	4417	1.1	0.4	1.0
			He I	4471	6.0	0.8	5.5
			He II	4686	5.5	0.8	5.3
			Ar IV	4712	2.9	0.3	2.8
			Ar IV	4740	3.3	0.3	3.2
			Hβ	4861	100.0	0.7	100.0
			He II	4922	1.2	0.5	1.2
			[O III]	4959	404.5	1.5	412.9
			[O III]	5007	1207.4	2.6	1244.6
			[N II]	5755	0.8	0.4	1.0
			He I	5876	10.0	1.6	11.9
			[K IV]	6102	0.2	0.1	0.2
			He II	6171	0.3	0.1	0.4
			[O I]	6300	4.8	0.1	6.0
			[S III]	6312	2.7	0.1	3.4
			O I	6363	1.5	0.1	1.9
			[Si II]	6371	0.2	0.1	0.3
			[N II]	6548	13.5	0.1	17.5
			Hα	6563	289.3	0.2	373.6
			[N II]	6584	40.7	0.5	52.6

Table A1 – *continued*

Id	$F_{H\beta}$	c_β Δc_β	Ion	λ (Å)	I_λ	ΔF_λ (%)	F_λ
			He I	6678	3.8	0.1	5.0
			[S II]	6717	3.0	0.1	4.0
			[S II]	6731	5.0	0.1	6.6
			He I	7065	9.7	0.1	13.3
			He I	7281	1.1	0.1	1.6
			[O II]	7320	6.4	0.1	9.0
			[O II]	7330	5.4	0.1	7.7
			[Ar III]	7751	3.3	0.2	4.9
			H I	8467	0.5	0.1	0.8
			[Cl III]	8500	0.6	0.1	0.9
			H I	8546	0.9	0.2	1.4
			[Cl II]	8579	0.2	0.1	0.3
			H I	859	0.7	0.2	1.2
			H I	8665	1.4	0.2	2.3
			N I	8680	0.7	0.2	1.1
			H I	8750	1.1	0.2	1.9
			H I	8862	1.3	0.2	2.2
			H I	9015	1.5	0.2	2.6
			[S III]	9069	12.7	0.2	22.0
			He I	9210	0.3	0.1	0.6
			H I	9229	2.0	0.2	3.6
			He I	9526	32.4	0.5	59.3
			H I	9546	2.5	0.3	4.6
			H I	10049	2.5	0.1	4.8
F1-10	1.715	0.306 ±0.022	He I	3734	32.2	8.8	26.4
			H I	3889	49.9	8.0	42.2
			[Ne III]	3968	25.3	8.3	21.7
			Hγ	4340	59.4	8.8	54.3
			O II	4349	22.2	9.7	20.3
			[O III]	4363	9.8	8.3	8.9
			[Fe II]	4413	19.1	14.1	17.6
			Hβ	4861	100.0	4.0	100.0
			[O III]	4959	246.7	4.1	251.0
			[O III]	5007	749.0	5.7	768.5
			[N I]	5198	4.9	2.3	5.2
			[Fe II]	5477	2.3	2.6	2.5
			[Fe II]	5496	2.0	2.5	2.2
			[Cl III]	5518	1.6	2.9	1.8
			[Fe II]	5582	460.3	5.7	517.7
			He I	5876	11.0	1.1	12.8
			[O I]	6300	4.7	1.1	5.7
			[N II]	6548	73.5	4.0	90.8
			Hα	6563	288.9	4.0	357.8
			He I	7065	5.4	1.5	7.1
			[Ar III]	7135	9.1	1.3	11.9
			[Fe II]	7220	7.7	1.3	10.2
			[O II]	7330	11.9	1.3	15.9
F1-13	4.359	0.423 ±0.010	H I	3657	3.8	11.1	2.8
			[O II]	3729	11.2	3.8	8.5
			H11	3771	10.6	4.9	8.2
			He I	3806	11.9	3.8	9.2
			[Ne III]	3868	25.2	2.8	19.8
			Hγ	4340	64.2	3.8	56.6
			O II	4349	8.4	3.5	7.4
			[O III]	4363	10.0	3.5	8.8
			Hβ	4861	100.0	1.9	100.0
			[O III]	4959	216.6	2.7	221.7
			[O III]	5007	643.8	3.8	666.7
			He I	5876	9.7	3.1	11.9
			[N II]	6548	2.1	0.5	2.8
			Hα	6563	289.7	1.1	389.3
			[N II]	6584	6.3	0.3	8.5
			He I	6678	3.5	0.4	4.8
			He I	7065	6.2	0.5	9.0
			[Ar III]	7135	9.3	0.4	13.5
			[O II]	7320	1.3	0.6	2.0
			[O II]	7330	1.7	0.5	2.6
			Si I	7538	4.2	0.4	6.5
			[Ar III]	7751	1.8	0.7	2.9
			[Cr II]	8000	1.4	0.7	2.3
			N I	8703	2.6	0.3	4.6
			N I	8712	7.8	0.5	14.0
			H I	9229	2.3	0.4	4.5
			[S III]	9069	7.8	0.5	14.8
			He I	9526	19.3	0.7	38.8
			H I	9546	2.1	0.4	4.2
			[C I]	9850	3.9	0.7	8.3
F1-14	15.01	0.403 ±0.004	[O II]	3729	17.2	2.1	13.2
			He I	3734	12.3	1.3	9.5
			He I	3785	1.4	1.5	1.1
			H I	3798	2.6	1.9	2.0
			He I	3872	37.6	1.2	29.9
			H I	3889	11.1	0.7	8.9
			[Ne III]	3968	29.4	1.2	23.9
			He I	4009	5.3	0.8	4.4
			Hδ	4100	32.5	1.1	27.3
			Hγ	4340	61.6	1.3	54.7
			[O III]	4363	10.7	0.7	9.5
			He I	4471	6.3	0.7	5.7
			[Fe II]	4874	1.5	0.3	1.5
			Hβ	4861	100.0	0.8	100.0
			He II	4922	1.8	0.3	1.8
			[O III]	4959	300.0	1.4	306.9
			[O III]	5007	889.7	2.5	920.1

Table A1 – *continued*

Id	$F_{H\beta}$	c_β Δc_β	Ion	λ (Å)	I_λ	ΔF_λ (%)	F_λ
			He I	5016	2.7	0.3	2.8
			[Fe II]	5582	33.3	0.6	38.8
			[N II]	5755	0.2	0.2	0.2
			He I	5876	9.8	0.4	11.9
			[O I]	6300	1.3	0.1	1.7
			[S III]	6312	0.6	0.0	0.8
			[O I]	6363	0.6	0.1	0.7
			[N II]	6548	6.1	0.1	8.1
			Hα	6563	289.5	0.4	383.7
			[N II]	6584	18.7	0.2	24.9
			He I	6678	4.4	0.2	5.9
			[S II]	6717	2.0	0.2	2.7
			[S II]	6731	3.5	0.2	4.8
			[Fe II]	6946	1.4	0.1	1.9
			He I	7065	8.5	0.2	12.0
			[Ar III]	7135	12.3	0.2	17.5
			He I	7281	1.3	0.2	1.9
			[O II]	7320	3.5	0.1	5.1
			[O II]	7330	2.8	0.2	4.0
			[Ar III]	7751	2.5	0.2	3.9
			H I	8598	0.8	0.2	1.3
			H I	8665	1.3	0.2	2.2
			H I	8750	0.8	0.2	1.5
			H I	8862	1.3	0.2	2.4
			H I	9015	1.5	0.1	2.7
			[S III]	9069	14.1	0.2	25.8
			H I	9229	1.9	0.2	3.6
			[S III]	9530	32.7	0.4	63.7
			H I	9546	2.2	0.3	4.3
			He I	10031	1.6	0.1	3.2
			H I	10049	3.2	0.2	6.6
F1-15	12.75	0.448 ± 0.005	[O II]	3726	28.9	1.3	21.6
			[Ne III]	3868	4.6	1.1	3.6
			H I	3889	7.5	1.2	5.8
			[Ne III]	3968	13.4	1.3	10.6
			He I	4009	3.1	1.0	2.5
			Hδ	4100	27.9	1.3	23.0
			O II	4157	3.7	0.7	3.1
			Hγ	4340	56.6	1.2	49.6
			[O III]	4363	2.5	0.6	2.2
			He I	4471	5.5	0.6	5.0
			Hβ	4861	100.0	1.0	100.0
			[O III]	4959	105.2	1.0	107.9
			[O III]	5007	311.5	1.7	323.3
			He I	5016	2.1	0.4	2.1
			[N II]	5755	1.4	0.1	1.7
			[O I]	6300	1.1	0.1	1.5
			[S III]	6312	0.6	0.1	0.8
			[Si II]	6347	0.3	0.2	0.3
			[O I]	6363	0.3	0.1	0.4
			[N II]	6548	26.8	0.3	36.6
			Hα	6563	289.8	0.8	396.4
			[N II]	6584	80.5	0.5	110.5
			He I	6678	3.9	0.2	5.4
			[S II]	6717	1.6	0.3	2.2
			[S II]	6731	3.0	0.3	4.2
			He I	7065	8.9	0.2	13.1
			[Ar III]	7135	11.4	0.3	16.9
			He I	7281	1.0	0.2	1.6
			[O II]	7320	16.9	0.3	25.7
			[O II]	7330	14.3	0.3	21.9
			[Ar III]	7751	2.6	0.3	4.2
			H I	8272	0.3	0.2	0.5
			O I	8447	1.8	0.2	3.2
			H I	8665	1.4	0.2	2.6
			H I	8750	2.1	0.2	3.9
			H I	8862	1.7	0.3	3.3
			H I	9015	1.7	0.2	3.4
			[S III]	9069	16.8	0.3	33.0
			H I	9229	2.5	0.3	4.9
			He I	9526	41.5	0.4	87.1
			[C I]	9850	0.9	0.2	2.0
			H I	10049	2.7	0.2	6.1
F1-16	16.54	0.409 ±0.005	He I	3806	4.0	0.9	3.1
			H I	3835	4.9	0.5	3.9
			[Si II]	3863	3.6	0.6	2.9
			[Ne III]	3868	42.3	1.3	33.6
			[Ne III]	3968	32.4	1.1	26.3
			Hδ	4100	29.4	1.3	24.6
			C II	4270	2.9	0.6	2.5
			Hγ	4340	59.2	1.1	52.5
			[O III]	4363	10.8	0.7	9.6
			He I	4471	6.5	1.0	6.0
			Ar IV	4711	1.5	0.8	1.4
			Ar IV	4740	1.6	0.7	1.6
			S II	4792	1.9	0.5	1.9
			He I	4922	1.5	0.7	1.5
			Hβ	4861	100.0	0.9	100.0
			He I	4922	1.5	0.7	1.5
			[O III]	4959	286.0	1.6	292.6
			[O III]	5007	850.3	2.7	879.7
			He I	5016	2.5	0.9	2.6
			[Fe II]	5582	29.8	0.3	34.8
			[N II]	5755	0.7	0.1	0.8
			He I	5876	10.3	0.2	12.6
			[O I]	6300	2.9	0.1	3.7

Table A1 – *continued*

Id	$F_{H\beta}$	c_β Δc_β	Ion	λ (Å)	I_λ	ΔF_λ (%)	F_λ
			[S III]	6312	1.0	0.1	1.2
			[O I]	6363	1.1	0.1	1.4
			He II	6406	0.2	0.1	0.3
			C II	6454	0.1	0.1	0.1
			[N II]	6548	11.8	0.1	15.7
			Hα	6563	289.5	0.5	385.3
			[N II]	6584	35.2	0.2	46.9
			He I	6678	4.0	0.1	5.4
			[S II]	6717	1.9	0.1	2.6
			[S II]	6731	3.4	0.1	4.6
			He I	7065	11.7	0.1	16.6
			[Ar III]	7135	15.2	0.2	21.9
			He I	7281	1.0	0.1	1.4
			[O II]	7320	7.7	0.1	11.2
			[O II]	7330	6.2	0.2	9.2
			[Ni II]	7378	0.6	0.2	0.9
			[Ar III]	7751	3.3	0.1	5.1
			H I	8467	1.8	0.1	3.0
			H I	8545	0.6	0.1	1.0
			H I	8598	0.8	0.1	1.4
			[C I]	8727	0.5	0.1	0.9
			H I	8750	1.1	0.1	2.0
			H I	8862	1.6	0.2	3.0
			H I	9015	2.0	0.2	3.6
			[S III]	9069	17.6	0.2	32.6
			H I	9229	2.7	0.2	5.1
			He I	9526	31.9	0.5	62.8
			H I	9546	2.5	0.2	4.8
			H I	10049	3.0	0.3	6.3
F1-20	13.37	0.531 ±0.005	He I	3478	5.1	0.1	3.4
			[O II]	3726	9.6	0.5	6.8
			[Ne III]	3868	32.3	3.4	23.9
			H I	3889	9.8	1.1	7.3
			[Ne III]	3968	15.4	3.1	11.7
			He I	4026	5.3	0.1	4.1
			Hδ	4100	28.5	3.5	22.6
			[Fe II]	4177	15.0	1.5	12.2
			Hγ	4340	54.3	2.2	46.4
			[O III]	4363	4.5	1.2	3.8
			He I	4471	5.7	0.7	5.1
			Hβ	4861	100.0	0.9	100.0
			He I	4922	1.3	0.1	1.3
			[O III]	4959	269.7	1.5	277.7
			[O III]	5007	800.4	2.5	836.2
			He I	5016	2.9	0.1	3.1
			[N I]	5200	0.6	0.1	0.7
			C IV	5802	0.7	0.2	0.9
			He I	5876	14.6	0.2	18.9
			[O I]	6300	2.8	0.2	3.8
			[S III]	6312	1.5	0.2	2.1
			[O I]	6363	1.1	0.2	1.5
			[N II]	6548	10.4	0.2	15.0
			Hα	6563	290.4	0.8	420.7
			[N II]	6584	32.6	0.3	47.4
			He I	6678	4.0	0.2	6.0
			[S II]	6717	1.4	0.2	2.0
			[S II]	6731	2.0	0.2	3.0
			He I	7065	11.8	0.2	18.7
			He I	7065	13.1	0.2	20.6
			[Ar III]	7135	15.3	0.3	24.4
			He I+[Fe II]	7281	1.4	0.2	2.3
			[O II]	7320	8.6	0.2	14.2
			[O II]	7330	7.0	0.2	11.5
			[Ar III]	7751	3.4	0.2	6.0
			N I	8184	0.2	0.1	0.3
			N I	8193	0.2	0.1	0.4
			H I	8359	0.3	0.2	0.7
			H I	8545	1.1	0.2	2.3
			H I	8595	0.5	0.2	1.0
			H I	8665	1.4	0.2	2.8
			H I	8750	1.1	0.2	2.3
			He I+[Fe II]	8830	5.2	0.2	11.2
			H I	8862	1.3	0.2	2.8
			He I	8966	2.9	0.2	6.3
F1-21	9.045	0.465 ±0.006	[O II]	3726	13.4	2.5	9.9
			He I	3872	23.8	2.5	18.3
			H I	3889	10.8	2.0	8.3
			[Ne III]	3968	10.5	2.5	8.3
			Hδ	4100	28.7	1.8	23.5
			Hγ	4340	65.4	0.3	57.0
			[O III]	4363	7.2	1.6	6.3
			[Fe II]+[O II]	4416	3.6	1.6	3.2
			O II	4673	3.9	1.8	3.7
			Hβ	4861	100.0	1.3	100.0
			He I	4922	1.8	0.7	1.9
			[O III]	4959	185.1	1.3	189.9
			[O III]	5007	542.5	2.5	564.0
			He I	5876	16.1	0.6	20.1
			[S III]	6312	2.2	0.8	2.9
			[N II]	6548	8.9	0.3	12.3
			Hα	6563	289.9	0.9	401.4
			[N II]	6584	26.7	0.4	37.1
			He I	6678	4.6	0.3	6.4
			[S II]	6717	1.3	0.3	1.8
			[S II]	6731	2.3	0.4	3.2
			He I	7065	9.6	0.4	14.3

Table A1 – *continued*

Id	$F_{H\beta}$	c_β Δc_β	Ion	λ (Å)	I_λ	ΔF_λ (%)	F_λ
			[Ar III]	7135	10.1	0.3	15.2
			[O II]	7320	8.6	0.4	13.4
			[O II]	7330	7.2	0.3	11.1
			[Ar III]	7751	2.3	0.4	3.9
			[C I]	8727	0.8	0.4	1.5
			H I	8750	1.4	0.4	2.6
			H I	8862	1.4	0.3	2.8
			[S III]	9069	15.7	1.2	31.7
			H I	9229	2.4	0.8	5.0
			[S III]	9530	32.6	1.0	70.5
			H I	9546	2.7	0.9	5.8
F1-22	0.324	0.743 ±0.079	[O II]	3726	141.8	15.0	87.7
			Hβ	4861	100.0	15.9	100.0
			[O III]	4959	374.5	20.6	390.4
			[O III]	5007	1130.7	27.1	1202
			[Fe II]	5582	2133.3	34.	2836
			[N II]	5755	5.6	19.2	7.8
			[Fe II]	5781	11.6	16.4	16.2
			[O I]	6300	55.2	6.5	87.2
			[O I]	6363	18.2	6.5	29.2
			Hα	6563	291.6	11.7	490.1
			[N II]	6584	39.7	7.0	67.1
			He I	6678	12.2	7.5	21.0
			[S II]	6717	18.7	10.7	32.6
			[S II]	6731	16.3	14.0	28.6
			He I	8777	38.5	7.5	109.8
			[S III]	9069	11.4	9.3	34.8
			[S III]	9530	24.9	8.9	84.9
			He I	10031	63.2	8.9	243.6
F2-3	1.209	0.456 ±0.025	H I	3669	29.0	4.4	21.2
			He I	3833	66.7	3.9	51.0
			[Si II]	3863	36.7	3.9	28.3
			[Ne III]	3868	77.6	4.4	59.9
			O II	4190	60.3	3.9	50.6
			Hγ	4340	90.0	4.5	78.6
			O II	4676	42.0	3.9	40.0
			He II	4686	44.2	4.5	42.2
			Hβ	4861	100.0	5.1	100.0
			[O III]	4959	191.1	4.6	196.0
			[O III]	5007	579.1	5.0	601.5
			He I	5876	11.2	4.4	13.9
			[O I]	6300	10.5	3.8	13.8
			[O I]	6363	5.6	1.2	7.5
			[N II]	6548	15.5	1.6	21.3
			Hα	6563	289.8	2.5	398.7
			[N II]	6584	48.9	4.3	67.4
			[S II]	6717	2.5	1.9	3.6
			[S II]	6731	3.7	1.4	5.2
			[K IV]	6792	3.2	1.5	4.6
			He I	7065	7.9	1.8	11.7
			[Ar III]	7135	6.8	1.8	10.1
			[O II]	7320	10.6	2.4	16.3
			[O II]	7330	9.2	1.9	14.1
			[S III]	9530	22.2	1.9	47.3
			[S III]	9069	11.3	1.8	22.4
F2-4	7.479	0.120 ±0.009	[O II]	3729	61.4	1.7	56.8
			He I	3872	11.6	0.9	10.8
			H I	3889	4.9	0.6	4.6
			He I	4009	31.0	1.1	29.3
			Hδ	4100	36.8	1.3	35.0
			Hγ	4340	87.6	1.9	84.6
			[O III]	4363	1.3	0.5	1.3
			[Fe II]	4457	6.4	0.8	6.3
			He I	4471	9.6	0.9	9.4
			Hβ	4861	100.0	1.9	100.0
			[O III]	4959	148.3	2.0	149.4
			[O III]	5007	316.9	3.0	320.1
			[N II]	5755	1.4	0.7	1.5
			He I	5876	19.0	0.5	20.1
			He II	5932	4.7	0.3	5.0
			[O I]	6300	2.3	0.2	2.5
			[O I]	6363	0.9	0.5	1.0
			[N II]	6548	29.4	0.6	32.0
			Hα	6563	287.7	0.9	313.0
			[N II]	6584	74.6	0.6	81.2
			He I	6678??	6.0	0.3	6.6
			He I	6678??	5.1	0.3	5.6
			[S II]	6717	2.4	0.2	2.6
			[S II]	6731	3.7	0.3	4.0
			[Fe II]	6746	1.9	0.3	2.1
			He I	7065	10.4	0.3	11.5
			[Ar III]	7135	11.2	0.4	12.5
			[O II]	7320	19.8	0.4	22.2
			[O II]	7330	12.6	0.4	14.2
			H I	8665	2.2	0.3	2.6
			H I	8750	1.9	0.3	2.3
			H I	8862	2.6	0.4	3.1
			[S III]	9069	25.7	0.4	30.8
			H I	9015	3.2	0.3	3.8
			[S III]	9530	63.6	0.5	77.6
			H I	9229	4.0	0.4	4.8
			H I	9546	5.8	0.3	7.0

Table A1 – *continued*

Id	$F_{H\beta}$	c_β Δc_β	Ion	λ (Å)	I_λ	ΔF_λ (%)	F_λ
F2-7	0.761	0.000 ±0.068	[Ne III]	3868	74.6	6.8	74.6
			H I	3889	147.2	9.7	147.2
			[Ne III]	3968	72.2	10.9	72.2
			He I	4120	436.7	14.1	436.7
			Hγ	4340	58.6	6.8	58.6
			[O III]	4363	46.2	6.2	46.2
			He II	4686	57.8	6.8	57.8
			Hβ	4861	100.0	9.3	100.0
			[O III]	4959	430.2	13.5	430.2
			[O III]	5007	1350.9	19.9	1350.9
			[Fe II]	5582	415.9	14.5	415.9
			[N II]	6548	9.1	6.4	9.1
			Hα	6563	159.4	10.1	159.4
			[N II]	6584	11.5	7.2	11.5
F2-10	8.334	0.110 ±0.008	[O III]	3729	37.3	1.1	34.7
			H I	3889	6.8	1.0	6.4
			He I	3806	3.4	1.0	3.1
			[Ne III]	3968	4.5	0.9	4.3
			Hδ	4100	18.6	1.2	17.8
			O II	4157	4.5	0.9	4.3
			[O III]	4363	61.1	1.6	59.1
			O II	4366	3.5	0.8	3.4
			Hβ	4861	100.0	1.7	100.0
			[O III]	4959	77.3	1.5	77.8
			[O III]	5007	214.7	2.0	216.7
			He I	5876	9.4	0.3	9.9
			[N II]	6548	13.6	0.3	14.7
			Hα	6563	287.7	0.9	310.7
			[N II]	6584	47.3	0.3	51.2
			He II	6683	2.6	0.2	2.9
			[S II]	6717	1.6	0.2	1.8
			[S II]	6731	1.7	0.3	1.8
			O II	6786	2.5	0.2	2.7
			[Ar V]	7006	0.8	0.2	0.9
			He I	7065	8.0	0.3	8.8
			[Ar III]	7135	4.9	0.3	5.4
			He I	7281	1.4	0.2	1.6
			[O II]	7320	16.5	0.5	18.3
			[O II]	7330	12.2	0.4	13.6
			H I	8268	1.1	0.3	1.3
			[S III]	9069	15.3	0.2	18.0
F2-11	2.456	0.000 ±0.014	He I	3926	23.1	1.2	23.1
			Hδ	4100	20.9	1.4	20.9
			Hγ	4340	46.9	1.7	46.9
			[O III]	4363	5.9	0.9	5.9
			Hβ	4861	100.0	2.3	100.0
			[O III]	4959	179.2	3.0	179.2
			[O III]	5007	505.3	5.4	505.3
			He I	5876	10.6	1.1	10.6
			Hα	6563	260.4	2.4	260.4
			[N II]	6584	3.0	0.8	3.0
			He I	6678	4.5	0.9	4.5
			[Ar III]	7135	10.7	1.4	10.7
			[S III]	9069	19.6	1.8	19.6
			He I	9526	26.4	6.0	26.4
F2-15	3.536	0.000 ±0.014	He I	3188	14.4	1.5	14.4
			H I	3734	5.7	1.1	5.7
			He I	3872	35.8	1.8	35.8
			Hγ	4340	60.2	2.3	60.2
			[O III]	4363	7.1	1.2	7.1
			N II	4780	10.8	1.6	10.8
			Hβ	4861	100.0	2.9	100.0
			He I	4922	4.3	1.3	4.3
			He I	5048	13.1	1.8	13.1
			[Fe III]	5412	3.1	1.5	3.1
			[O III]	4959	264.6	4.7	264.6
			[O III]	5007	834.8	5.6	834.8
			He I	5876	11.3	0.7	11.3
			Hα	6563	273.8	1.1	273.8
			[N II]	6584	7.0	0.8	7.0
			He I	6678	3.0	0.6	3.0
			He I	7065	4.9	0.6	4.9
			[Ar III]	7135	9.1	0.5	9.1
			H I	8750	19.9	1.4	19.9
			[S III]	9069	4.8	0.9	4.8